

# VERTICAL POSITION ERROR BOUNDING FOR INTEGRATED GPS/BAROMETER SENSORS TO SUPPORT UNMANNED AERIAL VEHICLE (UAV)

Jinsil Lee, Eunjeong Hyeon, Minchan Kim, Jiyun Lee  
Korea Advanced Institute of Science and Technology

**Keywords:** *Vertical position error bounding, UAV, Global Positioning System (GPS), Barometer, Weighted Least Square based RAIM*

## Abstract

*This study developed a method for integrity monitoring and derives Vertical Position Levels (VPLs) when Unmanned Aerial Vehicles (UAVs) use Global Positioning System (GPS) and a barometric altimeter for their navigation. To do this, we defined statistical error bounds of GPS pseudorange and barometer using experimental data. In addition, the nominal bias of range residuals from the barometer was considered by applying them when developing Weighted Least-Square (WLS) based Receiver Autonomous Integrity Monitoring (RAIM) algorithm. The results demonstrate that sensor integration improves availability by reducing VPLs than those of the case that only GPS was used in both fault-free and faulty condition.*

## 1 Introduction

As the number of autonomous Unmanned Aerial Vehicle (UAV) applications increases, reliable navigation sensors are becoming vital to enabling UAVs to conduct operations with minimal human intervention. One of the key system requirements that enable UAVs to coexist in non-segregated airspace with manned aircraft or other UAVs is navigation integrity. Integrity provides an assurance on a user position that the position error will not exceed predefined error limits due to undetected navigation system faults [1]. In the Global Navigation Satellites System (GNSS) context, several techniques to monitor system integrity

have been developed in previous researches. One of those methods is the receiver autonomous integrity monitoring (RAIM) [2], [3]. RAIM is a self-contained GNSS receiver-based integrity monitoring method utilizing onboard navigation sensor measurements. Therefore, RAIM does not need any external supports, which makes it a better integrity monitoring technology for UAVs compared to other ground-based integrity monitoring systems.

Various kinds of RAIM techniques have been proposed. One of the most prevalent and real-time based RAIM method is the Weighted Least Square (WLS) based RAIM. The WLS RAIM was proposed for supporting differential GPS based precision approach by Walter and Enge [4]. This technique exploits both the redundant measurements and the a-priori weighting information for each measurement to check the consistency of an overdetermined solution. Thus, if future multi-constellation GNSS and multi-sensor based navigation system are to offer more ranging signals, the WLS RAIM would fulfill more stringent navigation integrity requirements than the current performance level. Also, thorough understanding of a-priori weighting information for each different ranging source would be a key requirement for the WLS RAIM.

However, there are not many researches yet on the investigation of the performance of WLS

RAIM applied to multi-sensor based navigation systems; especially for commercial UAVs, which use relatively low cost sensors compared to civil aircraft. This work aims to evaluate the vertical navigation performance of UAVs from an integrity standpoint by adopting and modifying the proposed WLS RAIM algorithm when unaided Global Positioning System (GPS) and barometer are integrated as navigation sensors. For the integrity evaluation, fault detection test is conducted, and vertical protection levels (VPLs) are derived under both fault-free and faulty conditions. For the VPL computation, overbounded error models were derived for each navigation sensor that widely used for commercial UAVs. Finally, performance evaluation is conducted by comparing simulated VPLs for each sensor integrated scenarios.

This paper is organized as follows. Section 2 introduces the procedure for nominal measurement error and nominal bias bounding for both GPS and a barometer sensor to be used for the WLS RAIM in the following Section 3. Section 3 recalls the WLS RAIM concept and algorithms proposed in [4], and modified VPL formulation is introduced. The WLS RAIM algorithms are applied with modification to our simulations to conduct fault detection test and to compute VPLs for GPS/barometer integrated scenario under fault-free and faulty conditions. The simulation studies and simulated VPLs are shown in Section 4. The conclusion is drawn in Section 5.

## 2 Methodology for nominal measurement error bounding

### 2.1 Single-Frequency GPS Nominal Pseudorange Error Modeling

#### 2.1.1 Residual Ionospheric Error Modeling

The ionosphere is the major error source that affects positioning accuracy of single-frequency GPS users. To mitigate and characterize the ionospheric delay, Klobuchar ionospheric parameters [5] are being broadcast by GPS satellites. The model significantly reduces the effect of the ionospheric delay, but residual ionospheric delay remains. To gather the residual ionospheric delay dataset, nominal ionospheric delays observed in Korean region were used for modeling the bounded error model. Five nominal days in 2014 were chosen based on space weather indices, Planetary K (Kp) and Disturbance storm time (Dst) [6]. Ionospheric delays were obtained from the Long Term Ionospheric Anomaly Monitoring (LTIAM) software package [6]. Residual delays were computed by taking difference between the software-estimated ionospheric delays and Klobuchar model predicted delays.

To derive a bounded residual ionospheric delay model, residual delays are divided into 9 bins of elevation. Second, the mean ( $\mu$ ) and the standard deviation ( $\sigma$ ) of residual delays in each bin are computed and used to normalize the residual delays. Fig. 1 shows the folded Cumulative Distribution Function (CDF) [7] distribution of normalized residual delays on a logarithmic scale. It is clearly seen that the distribution (the dotted curve) has non-Gaussian tails. Thus, the normalized distribution was bounded by applying inflation factor of 1.3 as shown in Fig. 1 with red solid curve.

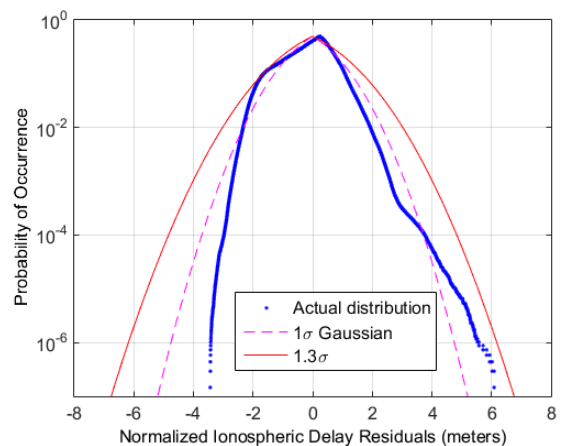


**Fig. 1.** The folded CDF bounding for ionospheric delay residuals. The distribution of residuals is well bounded by a Gaussian distribution with an inflation factor of 1.3.

Fig. 2 shows means, standard deviations and determined  $\sigma_{\text{residual iono}_{ob}}$  for each bin of elevation. Finally, the resulting  $\sigma_{\text{residual iono}_{ob}}$  was applied to form the pseudorange error model.

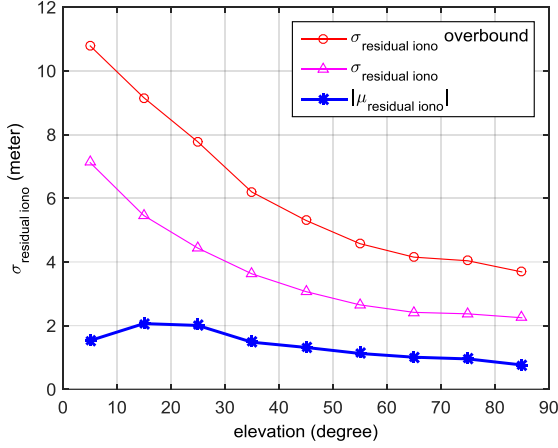


**Fig. 2. The mean (blue star), the standard deviations (purple triangle), and their overbound sigmas (red circle) of ionospheric delay residuals for each elevation level.**

### 2.1.2 Error Models for Troposphere, Airborne Multipath And Noise and Satellite Clock/Ephemeris

Residual tropospheric delay is modeled as (1) as a function of satellite elevation [8].

$$\sigma_{\text{tropo}} = \sigma_{\text{TVE}} \cdot m(el) \quad (1)$$

where  $\sigma_{\text{TVE}} = 0.12m$  and

$$m(el) = \frac{1.001}{\sqrt{0.002001 + \sin^2(el)}} \quad (2)$$

For multipath error, the standard airborne multipath model proposed in [8] is used which is given by:

$$\sigma_{\text{MP}}(el) = 0.13 + 0.53 \exp(-el / 10 \text{ (deg)}) \quad (3)$$

Previous study showed that the model (3) bounds the multipath error for the UAV based on UAV flight test data collected at the flight altitude of 40m, which is lower than that of manned aircraft, but well within the flight region of UAVs [9]. Therefore, it is reasonable to use the standard multipath error model in this study.

For receiver noise model, standard model from [8] is applied:

$$\sigma_{\text{Noise}}(el) = 0.15[m] + 0.43[m] \exp(-el / 6.9[\text{deg}]) \quad (4)$$

Finally, airborne multipath is determined as (5) [9].

$$\sigma_{\text{air}} = \sqrt{\sigma_{\text{mp}}^2 + \sigma_{\text{noise}}^2} \quad (5)$$

User Range Accuracy (URA) values which are bounded standard deviation of satellite clock/ephemeris residual errors can be obtained from navigation messages. In this study, the URA value of 2.4m, which is the most common value broadcast from satellite, is applied [10].

### 2.1.3 Total Pseudorange Residual Error Models Applied For Simulation

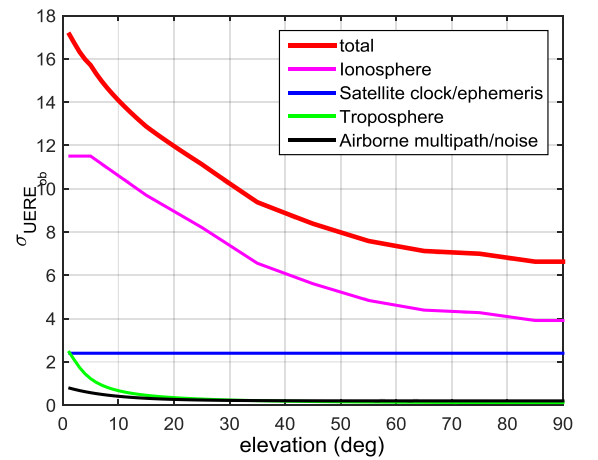


**Fig. 3. Total pseudorange residual error models applied for simulation**

Fig. 3 shows the bounded pseudorange residual error models applied to form a weighting matrix in a WLS filter and WLS RAIM which will be discussed later in chapter 3.

## 2.2 Nominal Error Bounding For Barometer Sensor

### 2.2.1 Barometer Basics

A barometer is a device measuring altitude using a pressure sensor. The principle of a barometer is based on the fact that atmospheric pressure is varied according to altitude. Barometers measure atmospheric pressure using their pressure sensors and convert the pressure measurements to the altitude of their location using the equation (6) [11].

$$\hat{h}_c = \frac{T_0}{\lambda} \left[ 1 - \left( \frac{P_m}{P_0} \right)^{\lambda R/g} \right] \quad (6)$$

### 2.2.2 Barometer Measurements

To derive statistics of barometer measurement errors in nominal condition, barometer data is collected at the precisely known position and is compared with the true altitude. The data was collected at the known location of altitude of 97.7582 meters. For the data collection, barometer embedded in the Pixhawk controller were updated every 1s for 18 hours. During the experiment, the barometer kept to be static at the outdoor condition.

For computing precise altitude from barometer, Mean Sea Level (MSL) and temperature corrections should be applied. For the MSL correction, we applied the MSL pressure and temperature data from the nearest weather station [12].

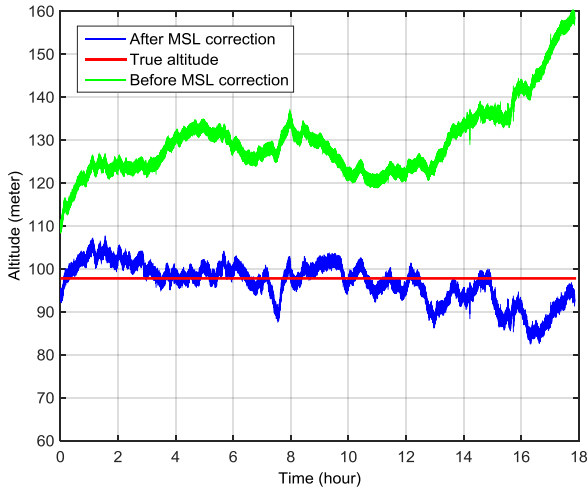


**Fig. 4.** Barometer measurements before applying MSL correction (a green line), and after the correction (a blue line). The true altitude was 97.7582 meters (a red line).

Fig. 4 shows the barometer measurements before applying MSL correction (the green line) and after applying MSL correction (the blue line). After correcting MSL pressure and temperature, the measurements level becomes much closer to the true altitude value. In addition, the variance of the data becomes smaller, because pressure and temperature would be varied in day and night.

However, even though we corrected the MSL pressure and temperature, the barometer measurements have an uncorrected bias about 1.009 meters with respect to the true altitude. This might be induced from the pressure variation error [12] caused by the difference

between the actual pressure versus altitude relationship and the theoretical relationship as the equation (6). This type of biases can be considered as ‘nominal bias’. The nominal bias bound which could appear random but affect user in the same way [13]. In order to be more realistic, barometer measurement models need to take into account this nominal bias. The techniques to deal with the nominal bias in the barometer is discussed in the following section.

### 2.2.3 CDF Bounding: Adaptation to Nominal Bias

In order to describe the statistics of barometer measurement errors, we assumed the errors have a Gaussian distribution with the mean value as a nominal bias, 1.009 meters. Then, we normalized the measurement errors with their mean and standard deviation ( $\sigma = 4.5221m$ ). With the normalized measurement errors, we implemented one-minus cumulative distribution function (1-CDF) bounding technique [7] without considering sign of errors. By inflating standard normal distribution until the inflated distribution bounds the measurement error distribution, bounded standard deviations are determined to the the probability of  $10^{-5}$ .

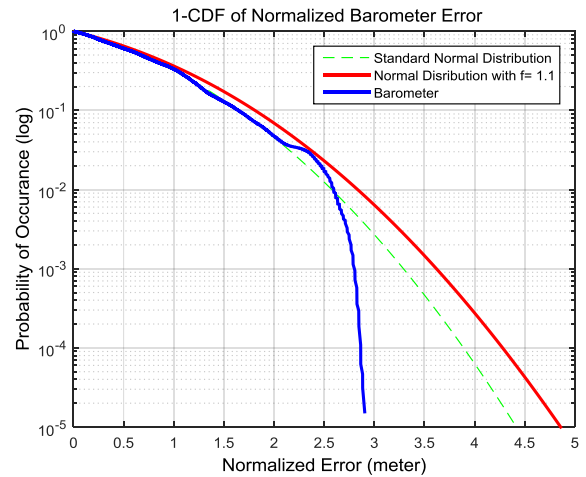


**Fig. 5.** The 1-CDF of the standard normal distribution (green dashed line), the normal distribution with 1-sigma = 1.1 (red solid line), and the barometer measurement errors (blue solid line).

Fig. 5 presents the results of the 1-CDF bounding for the barometer measurement errors. In Fig. 5, the distribution of measurement errors do not perfectly follow the standard normal distribution. Therefore, the inflation factor

$f = 1.1$  is determined. Finally, the barometer measurement error could be overbounded by:

$$\sigma_{\text{overbound,baro}} = (4.5221m) \cdot f = 4.9743m \quad (7)$$

### 3 WLS RAIM Based Fault Detection and VPL Computation

#### 3.1 WLS RAIM Concept and Algorithm

This study adopted the concept of WLS RAIM, which was proposed for GPS-based precision approach by Walter and Enge [4], to perform a multi-sensor based navigation fault detection and to compute VPLs. This section 3.1 reviews the concept of WLS RAIM as described in the literature [4]. The WLS RAIM is a snapshot-based monitoring scheme which can detect a single measurement fault and compute protection levels. It monitors consistency of measurement residuals based on the navigation filter estimated position.

The measurement residuals are converted into a position error domain as (8).

$$\Delta\rho = H \cdot \Delta X + \varepsilon \quad (8)$$

where  $\Delta\rho$  is the measurement residual,  $H$  is the geometry matrix,  $\Delta X$  is the position and receiver clock error, and  $\varepsilon$  is the measurement error vector.  $\Delta X$  is then represented as (9).

$$\Delta X = (H^T \cdot W \cdot H)^{-1} \cdot H^T \cdot W \cdot \Delta\rho \quad (9)$$

where  $W$  is the inverse of the measurement covariance matrix. To test the goodness of the WLS fit, Weighted Sum of Squared Error (WSSE) is monitored defined as (10) [4].

$$\begin{aligned} WSSE &= \varepsilon^T \cdot W \cdot \varepsilon \\ &= (\Delta\rho - H\Delta X)^T \cdot W \cdot (\Delta\rho - H\Delta X) \\ &= \Delta\rho^T \cdot W \cdot (I - H(H^T \cdot W \cdot H)^{-1} H^T W) \Delta\rho \\ &= \Delta\rho^T \cdot S \cdot \Delta\rho \end{aligned} \quad (10)$$

Provided that  $\varepsilon$  follows a Gaussian distribution, WSSE is a central chi-squared distribution with  $(N-4)$  degrees of freedom under fault-free conditions [4]. When one of measurements contains bias, the aforementioned chi-square

becomes non-central chi-square that has non-centrality parameter ( $\lambda$ ) resulting from the bias as described in Fig. 6. With a given probability false alert ( $P_{fa}$ ), the threshold is chosen. Then, the noncentrality parameter  $\lambda$  can be determined based on a probability of missed detection ( $P_{md}$ ). The  $\lambda$  is converted into position domain, then the upper bound position error resulting from the minimum detectable bias is determined. Finally, VPL under faulty condition, referred as  $VPL_{FD}$ , is obtained as shown in Fig. 6.

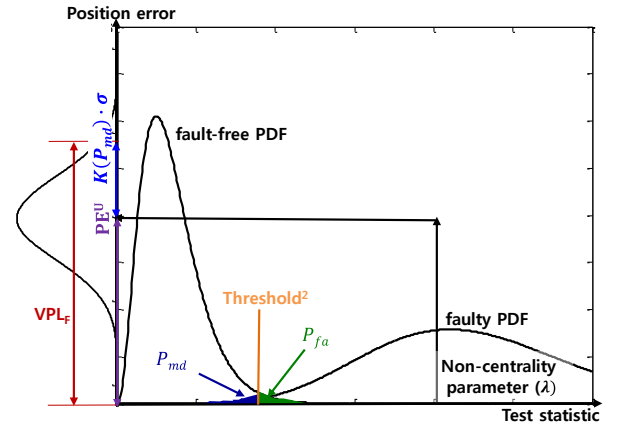


**Fig. 6. The probability density function for fault-free test statistics (left) and faulty test statistics (right)**

#### 3.2 Integration of a Barometer to the GPS Based WLS RAIM

##### 3.2.1 WLS RAIM Formulation of Barometer-Aided GPS Case

To formulate the WLS RAIM algorithm with an additional barometer sensor, barometer measurement is assumed as an additional satellite placed along the vertical direction without clock bias formed as (11), (12) and (13) [11].

$$\begin{aligned} \Delta X_{\text{predicted}} &= (H_{GB}^T \cdot W_{GB} \cdot H_{GB})^{-1} \cdot H_{GB}^T \cdot W_{GB} \cdot \Delta\rho_{GB} \end{aligned} \quad (11)$$

where

$$W_{GB}^{-1} = \begin{bmatrix} \sigma_1^2 & 0 & \dots & 0 \\ 0 & \sigma_2^2 & \dots & 0 \\ \vdots & \dots & \ddots & 0 \\ 0 & 0 & \dots & \sigma_{\text{baro}}^2 \end{bmatrix} \quad (12)$$

$$H_{GB} = [H_{GPS}; H_{Baro}] \quad (13)$$

where  $H_{Baro} = [0 \ 0 \ 1 \ 0]$

GPS pseudorange residuals ( $\Delta\rho_G$ ) are formed by taking difference between measurement pseudorange and predicted pseudorange. The predicted pseudorange is generated by establishing the geometric range between the filter estimated position and known satellite ephemeris. Model estimated errors such as satellite clock bias, receiver clock bias and atmospheric errors are also considered to derive the predicted pseudorange. A barometer measurement residual is modeled as described in the section 2.2.2 to section 2.2.3.

### 3.2.2 Consideration of Nominal Bias in the Barometer Residual Error

The nominal bias is an upper bound on nominal, uncorrectable errors present on ranging signals. Most barometer measurements possess biases all the time, which is originated from the conversion from pressure to altitude. Since these biases occurred repeatedly but randomly, they can be considered nominal biases. However, when range residuals have nominal biases, RAIM algorithm need to be differentiated to the classical WLS RAIM method. There have been several researches to adapt nominal bias in pseudorange errors to the test statistics of WLS RAIM [14]. In this section, we developed an algorithm to adjust nominal bias only from the barometer residual error with the assumption that pseudorange residual errors of GPS measurements have zero-mean distribution.

We changed the range residual  $\Delta\rho$  as the equation (14), which a nominal bias term  $a$  is added only in the barometer component.

$$\Delta\rho(k) = \begin{bmatrix} \Delta\rho^{(1)}(k) \\ \vdots \\ \Delta\rho^{(2)}(k) \\ \Delta\rho^{baro}(k) \end{bmatrix} + \begin{bmatrix} 0 \\ \vdots \\ 0 \\ a \end{bmatrix} \quad (14)$$

where  $\Delta\rho^{(i)} \sim N(0, \sigma_i^2)$ , and  $\Delta\rho^{baro} \sim N(a, \sigma_{baro}^2)$

In the above equation,  $k$  represents a time epoch, and  $\Delta\rho$  is a range residual for each measurement. Then, the noncentrality

parameter  $\lambda$  of the distribution of fault-free test statistics becomes:

$$\lambda = \sum_{i=1}^{N-4} \frac{\mu_i^2}{\sigma_i^2} + \frac{a^2}{\sigma_{baro}^2} \quad (15)$$

$$= \frac{(1.0092m)^2}{(4.9743m)^2} = 0.0412$$

In the equation (15),  $N$  represents the number of range measurements from the satellite at a time epoch  $k$ . The range residuals from satellites are assumed to have zero mean, therefore,  $\mu_i = 0$  and only the barometer range bias remains as  $a = 1.0092m$ .

Consequently, as including the nominal biases, the distribution of WSSE which was the central chi-squared distribution in the fault-free condition is changed to non-central chi-squared distribution [14].

### 3.3 Modified VPL Formulation for the Barometer-Aided GPS Navigation System

In this section, we reformulated VPL equations to consider the nominal bias of the barometer measurements. The VPL equations we proposed here are based on the algorithm that Walter and Enge suggested [4].

#### 3.3.1 VPL from Barometer-Aided GPS Measurements under Fault-Free Condition

In this section, VPL under fault-free condition is formulated.  $VPL_{NF}$  is represented as (16):

$$VPL_{NF} = Q^{-1}(0.25P_{HMI})\sigma_v + A_{v,b}a \quad (16)$$

where  $A = (G^T W G)^{-1} G^T W$

$\sigma_v$  is the overbounded standard deviation of position error in vertical direction,  $A_{v,b}$  plays the role of converting nominal bias in the range domain into that in the vertical position domain, and  $P_{HMI}$  is a probability of Hazardous Misleading Information (HMI). In this study, 1/2 of the  $P_{HMI}$  is assumed to be allocated for the  $VPL_{NF}$ .

### 3.3.2 VPL from Barometer-Aided GPS Measurements under Faulty Condition

The worst bias ( $b_i^{worst}$ ), referred as Minimum Detectable Error (MDE), is determined from a non-centrality parameter  $\lambda$  using the equation (17) [15]. The worst bias computed for each measurement, and the one which makes the largest VPL is used for the VPL computation.

$$b_i^{worst} = \sqrt{\lambda / S_{ii}} \quad (17)$$

Then, the worst bias in the equation (17) is applied to calculate VPE upper bound,  $VPE^U$ , as the equation (18).

$$VPE_i^U = |A_{v,i}| b_i^{worst} \quad (18)$$

Finally, the equation calculating VPL under the faulty condition is expressed as the equation (19). In the equation (19), the nominal bias of the barometer residual errors is included, since  $b_i^{worst}$  is determined from the WSSE distribution adapting the nominal bias.

$$VPL_{FD} = \max_i \left( Q^{-1}(P_{MD}) \cdot \sigma_v + VPE_i^U \right) \quad (19)$$

## 4 Simulation Studies

### 4.1 WLS RAIM Based Fault Detection

For the simulation studies, data of GPS pseudorange measurements, satellite ephemeris and barometer altitude are collected during 15 hours. For the threshold determination, it is assumed that the UAV executes a vertical navigation approach according to approach procedures with vertical guidance I (APV-I). According to the International Civil Aviation Organization specification, probabilities related to the performance requirements for APV-I approach are selected [16]. Fig. 7 shows the results of fault detection test. Lines with dots show the test statistic computed from collected measurements. Solid lines represents corresponding thresholds determined based on  $P_{fa}$  and the number of satellites. It is shown that there is no test statistics which exceeds its threshold even though some of the test statistics

computed from barometer-aided GPS case have several peaks due to biases from barometer measurements. Thus, VPLs can be computed at all time during our simulation period.

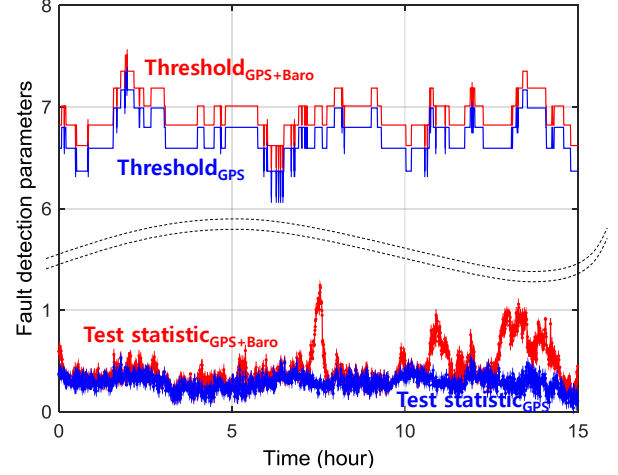


**Fig. 7 Threshold and test statistics for GPS (blue) and GPS/barometer integration (red)**

### 4.2 VPLs under Fault-Free Conditions

In the Fig. 8, VPLs for fault-free condition computed from (16) are presented in the upper graph, and the corresponding number of satellites is presented in the bottom graph. The results show that  $VPL_{NF}$  for the barometer-aided GPS scenarios have much smaller values compared to those for the GPS-only scenario, even though we adopted the nominal bias of the barometer to the VPL.

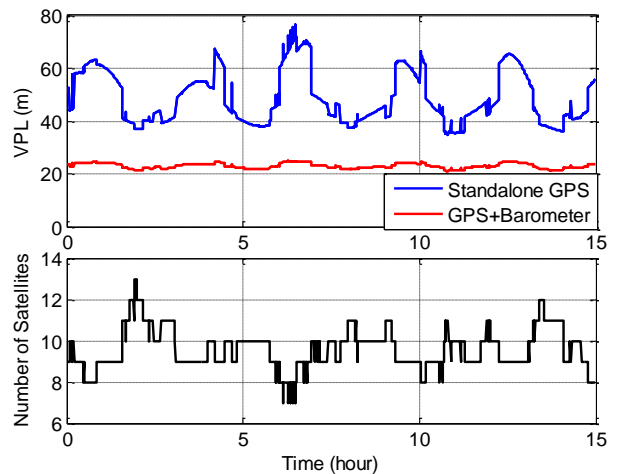
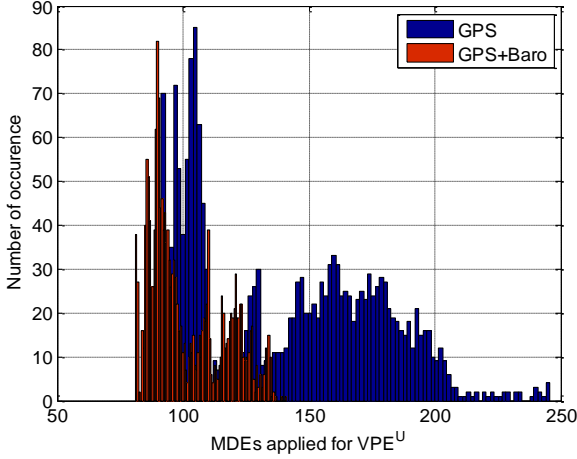


**Fig. 8. VPL performance comparison under fault-free condition. The bottom graph presents the number of GPS satellites over time.**

### 4.3 VPLs under Faulty Conditions

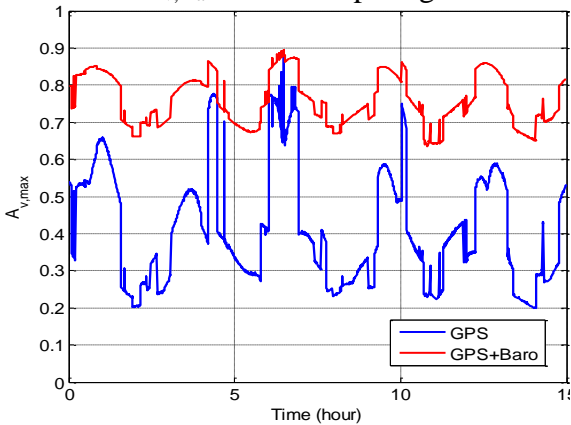
**4.3.1 VPL Performance of Barometer-Aided GPS Condition under Faulty Condition**

VPL under the faulty condition is simulated according to the algorithm we suggested in the section 3.3.2. Fig. 9 shows the histogram of the MDEs which are used when computing  $VPE^U$ . It is shown that the barometer-aided GPS case applies much smaller MDEs when computing  $VPE^U$ .



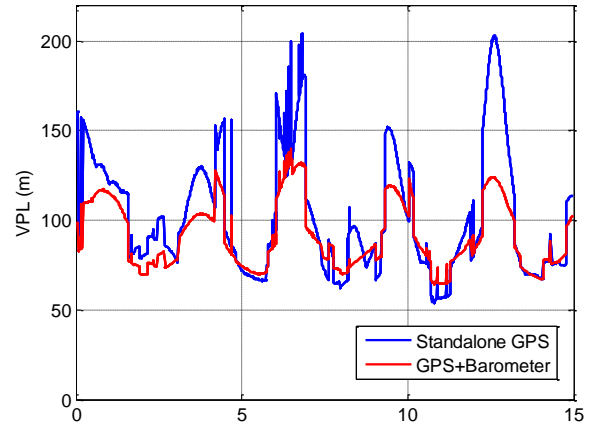
**Fig. 9. Comparison of MDEs for GPS-only case and barometer-aided GPS case.**

Fig. 10 represents  $A_{v,max}$ , which is chosen to maximize  $VPL_{FD}$  among  $A_{v,i}$  from all measurements. The  $A_{v,max}$  from the barometer-aided GPS case has higher value than those from GPS-only case all the time. It is noteworthy that all the  $A_{v,max}$  values from the barometer-aided GPS case are determined from  $A_{v, barometer}$ . This is because a vertical position error is more sensitive to errors in measurements coming from a vertical direction than others. Therefore,  $A_{v, barometer}$  is always selected as a  $A_{v,max}$  when computing  $VPE^U$ .



**Fig. 10.  $A_{v,max}$  for the GPS-only case (blue) and the barometer-aided GPS case (red) under faulty case.**

The simulated  $VPL_{FD}$  using the equation (19) are depicted in Fig. 11. Unlike the  $VPL_{NF}$ , overall trend for  $VPL_{FD}$  from GPS only is greater than  $VPL_{FD}$  from barometer-aided GPS. However, the opposite trend also can be found especially when  $VPL_{FD}$  for GPS is small. This is caused by large  $VPE^U$  of the barometer due to barometer geometry which is highly vulnerable to the vertical position error. Due to the conservative assumption of WLS RAIM that selects a worst geometry, the MDE values are reflected directed to the  $VPL_{FD}$ .



**Fig. 11. VPL performance of GPS-only case (blue) and barometer-aided GPS case (red) under faulty condition.**

**4.3.2 VPL Performance Improvement of Barometer-Aided GPS Condition under Faulty Condition**

In section 4.3.1, VPL of the barometer-aided GPS case under faulty condition is computed assuming that the barometer fault may occur with the same probability in both GPS and the barometer sensor. As a result, large  $VPE^U$  is applied to the final  $VPL_{FD}$ . In this section, this large  $VPE^U$  is mitigated by assuming unexpected fault (such as hardware malfunction, which is a rare or unreported event in barometers) will not occur in a barometer. This assumption might be reasonable for our simulation because we corrected other possible error sources such as MSL pressure and temperature for every minute.

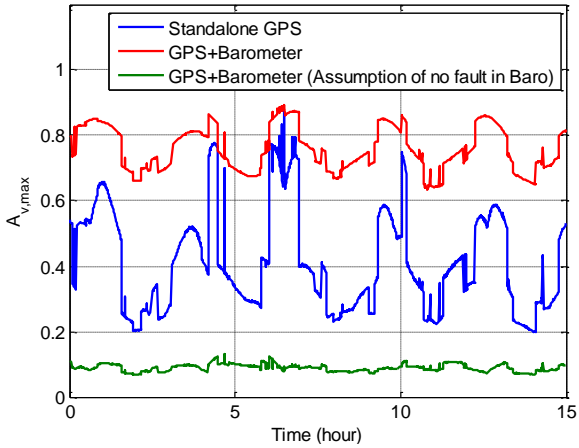


**Fig. 12.  $A_{v,max}$  comparison between each sensor integration scenarios (with assumption of no fault in barometer)**

The aforementioned assumption results in much smaller  $A_{v,max}$  as shown with green line in Fig. 12. The  $A_{v,max}$  is chosen by taking maximum value among  $A_{v,gps_i}$ . Finally, the modified  $VPL_{FD}$  result in Fig. 13 shows that the  $VPL_{FD}$  can be much less conservative.

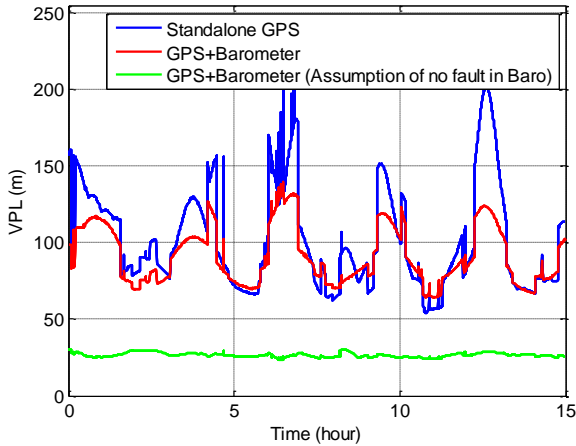


**Fig. 13.  $VPL_{FD}$  comparison between each sensor integration scenarios (with assumption of no fault in barometer)**

#### 4.3.4 VPL Performance Comparison of GPS-Only Condition to Barometer-Aided GPS Condition

In Fig. 14, it is shown that the integration of GPS and a barometer for vertical guidance provides better performance from an integrity point of view. However, the sensitivity of the VPL to test statistics (or MDE) should be carefully considered when adding a barometer under faulty conditions.

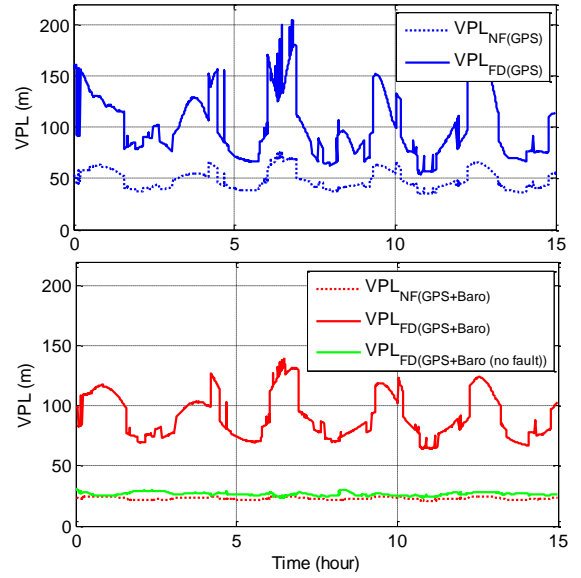


**Fig. 14. Comparison of VPL performance for GPS only case (blue) and GPS/barometer integration case (red) for both fault-free (dashed line) and faulty (solid line) conditions.**

## 5 Conclusions

In this paper, we derived the error bounds of both GPS pseudorange residuals, and barometer residual errors. A nominal bias was modelled for the barometer residual error. The bounded errors were applied to the WLS RAIM algorithm to detect measurement faults, and to attain VPLs for both the fault-free and faulty conditions. VPLs were compared between two sensor scenarios (the GPS-only case, and the barometer-aided GPS case).

The  $VPL_{NF}$  performance clearly shows that the barometer improved the level of the system availability in the vertical direction. For the  $VPL_{FD}$  case, the performance improvement was not significant in the barometer-aided scenarios. This is because the vertical position error is highly sensitive to barometer measurement faults, and thus the determined MDE is applied directly to the vertical position error bound. Additional analysis was conducted to mitigate the conservatism on VPL with the assumption that faults would not occur in a barometer, but only occur in one of the measurements from GPS. The assumption significantly lowered the conservatism on  $VPL_{FD}$ . However, when applying the assumption to operating UAVs, all the possible faulty scenarios (data transmission

loss, operating distance from the MSL/temperature reference station etc.) should be considered prior to operations. Additional barometer fault monitoring would be another solution for lowering the conservatism.

The results presented here were based on limited experimental conditions and data. Therefore, further investigations on sensor modelling under more diverse conditions are required. The computation of VPL for multi-sensor navigation systems would assist in the operation of UAVs which require precise and reliable vertical guidance. The determination of integrity levels through the computation of error bounds will allow the users to carry out missions with guaranteed safety levels.

## 6 Acknowledgments

This work was supported by the Institutes for startup KAIST (ISK).

## References

- [1] T. Walter, P. Enge, J. Blanch, and B. Pervan, "Worldwide vertical guidance of aircraft based on modernized gps and new integrity augmentations," *Proc. IEEE*, vol. 96, no. 12, pp. 1918-1935, Dec. 2008.
- [2] Brown, R. G. (1993). Receiver Autonomous Integrity Monitoring. *Global Positioning System Theory and Application*. B. W. Parkinson and J. J. Spilker Jr. Washington D.C., American Institute of Aeronautics and Astronautics 2: 143-186.
- [3] Brown, R. G. (1992), A baseline GPS RAIM scheme and a note on the equivalence of three RAIM methods, *Navigation*, Vol. 39 No. 3 pp. 101-116.
- [4] Walter, T., et al. Weighted RAIM for precision approach. In *Proceedings of the ION GPS-95*, Palm Springs, FL, 1995.
- [5] Klobuchar JA. Ionospheric time-delay algorithm for single-frequency GPS users. *IEEE Transactions on aerospace and electronic systems*. 1987, Vol. AES-23, No. 3, pp. 25-31.
- [6] S. Jung, and J. Lee, "Long-term ionospheric anomaly monitoring for ground based augmentation systems," *Radio Sci.*, vol. 47, no. rs4006, Jul. 2012.
- [7] DeCleene B. Defining Pseudorange Integrity – Overbounding. *Proceedings of the 13th International Technical Meeting of the Satellite Division of The Institute of Navigation*, Salt Lake City, UT, September 2000, pp. 1916-1924.
- [8] MOPS, WAAS. Minimum operational performance standards for global positioning system/wide area augmentation system airborne equipment. RTCA Inc. Document No. RTCA/DO-229B 6 (1999).
- [9] Kim, Minchan, Kim, Kiwan, Lee, Jiyun, Pullen, S., "High Integrity GNSS Navigation and Safe Separation Distance to Support Local-Area UAV Networks," *Proceedings of the 27th International Technical Meeting of The Satellite Division of the Institute of Navigation (ION GNSS+ 2014)*, Tampa, Florida, September 2014, pp. 869-878.
- [10] Heng, L., Gao, G.X., Walter, T., Enge, P. (2011) "Statistical Characterization of GPS Signal-In-Space Errors." *Proceedings of the 2011 International Technical Meeting of The Institute of Navigation*, San Diego, CA, pp. 312-319.
- [11] Shau-shiun J, Demoz G, Todd W, and Per E. Improving GPS-Based Landing System Performance using an Empirical Barometric Altimeter Confidence Bound. *IEEE Transactions on Aerospace and Electronic Systems*, Vol. 44, No. 1, pp 127-146, 2008.
- [12] Korea Meteorological Administration, Autonomous weather station, [http://www.kma.go.kr/weather/observation/ws\\_table\\_popup.jsp](http://www.kma.go.kr/weather/observation/ws_table_popup.jsp).
- [13] Todd W, Juan B, and Per E. Evaluation of Signal in Space Error Bounds to Support Aviation Integrity, *NAVIGATION, Journal of the Institute of Navigation*, Vol. 57, No. 2, pp 101-113, 2010.
- [14] Martineau A. Doctoral dissertation, Ecole Nationale de l'Aviation Civile, 2008.
- [15] Teunissen PJ. Minimal detectable biases of GPS data. *Journal of Geodesy*. 1998 Apr 1;72(4):236-44.
- [16] International Civil Aviation Organization (ICAO) International standards and recommended practices: Aeronautical telecommunications. Annex 10, Vol. I, Radio Navigation Aids, Section 3.7.2.4.1, ICAO.

## 7 Contact Author Email Address

The contact author to this paper is Jiyun Lee (jiyunlee@kaist.ac.kr)

## Copyright Statement

The authors confirm that they, and/or their company or organization, hold copyright on all of the original material included in this paper. The authors also confirm that they have obtained permission, from the copyright holder of any third party material included in this paper, to publish it as part of their paper. The authors confirm that they give permission, or have obtained permission from the copyright holder of this paper, for the publication and distribution of this paper as part of the ICAS proceedings or as individual off-prints from the proceedings.